

Coherent Control of Fano Resonances in a Macroscopic Four-Mirror Cavity

Nikhil Pramanik,¹ Krishna Chaitanya Yellapragada,² Suneel Singh,¹ and P. Anantha Lakshmi^{1,*}

¹*School of Physics, University of Hyderabad, Hyderabad, Telangana 500046, India*

²*Centre for Quantum Technologies, 3 Science Drive 2,
National University of Singapore, 117543, Singapore*

(Dated: April 16, 2019)

We demonstrate coherent control of optomechanically induced transparency and Fano resonances in a four mirror macroscopic optomechanical cavity, with two movable mirrors, each driven by an external mechanical pump. The variable control of the amplitude and phase of the coherent mechanical pumps provides a means of tuning the shape and nature of the Fano profiles. Further, our scheme shows the occurrence of tunable optomechanical features, even at very low mechanical driving field amplitudes, in macroscopic optomechanical cavities.

keywords: Four mirror, Fano resonance, optomechanically induced transparency, mechanical driving, optomechanical system

PACS numbers: 03.65.Ud , 03.67.-a, 42.50.Ar

I. INTRODUCTION

Quantum interference between different transition pathways gives rise to several interesting physical phenomena, such as Fano resonances [1], that have been observed in a variety of physical systems. For instance, in plasmonics, photons are allowed to travel through multiple transition pathways which interfere, thus making the occurrence of Fano line shapes quite common in such materials. Fano resonances have been observed in phonon interactions in solids [2, 3], electron transport in quantum wells/dots [4, 5], photonic crystals [6], coupled photonic microcavities [7, 8], plasmonic metamaterials [9], nanoparticles [10–13] and electromagnetic metamaterials [14–18].

Fano line shapes are also used in obtaining information on the interaction between nanoparticles with light [19–22], for local refractive index sensing applications [23], efficient confinement of light [24], surface enhanced Raman scattering (SERS) [25], generation of slow light [26], enhanced light transmission [27] and sensitive biosensors [28]. Fano interference is seen to play an important role in producing lasing without population inversion [29–32] and as a tool to probe decoherence [33–35] in the field of quantum optics and quantum information. Fano resonances have also been widely studied theoretically in hybrid optomechanical systems with distinct configurations [35–40]. More recently, Fano resonance and slow light is studied in the hybrid optomechanical system [41–43].

In the existing studies of cavity optomechanics, the optomechanical (OM) effects (that depend upon G^2) become significant only when the effective OM coupling parameter G is sufficiently large. This in turn requires extremely small sizes of mirrors and cavity arm lengths because the OM coupling parameter is inversely proportional to cavity length, size and weight (physical dimen-

sions) of the mirror. Obviously in macroscopic cavities i.e. for large cavity length, mirror size and weight, OM coupling G is very weak and hence it is not possible to observe OM effects for such small values of G .

In this work we propose a novel scheme that enables one to observe OM effects even in macroscopic cavities, i.e., even for negligible G . We study the occurrence of Fano resonances and the related phenomenon of optomechanically induced transparency (OMIT) by analyzing the fields generated at the anti-Stokes frequencies in a macroscopic cavity. By introducing coherent mechanical pump to act on two mirrors of the four mirror cavity, we show that optomechanical interaction can be enhanced, thus resulting in appearance of Fano resonances and OMIT features in the generated anti-Stokes signals. For suitable choice of the amplitude and phase of the mechanical driving fields and mirror oscillation frequencies, we demonstrate the occurrence of tunable double Fano resonance in cavity optomechanics and further identify the interfering contributions to the fields generated at anti-Stokes frequencies, from a detailed study.

The paper is organized as follows: In Sec. II we describe the system that is studied here together with necessary mathematical formulation and solutions for the dynamical evolution of different quantities of interest. In sec. III numerical results pertaining to the OMIT and the asymmetric Fano-like resonance induced by interference of two transition pathways are presented. We further show the generation of double Fano-like resonances for specific choice of the drive amplitudes and phases. A summary of results and conclusions are presented in sec. IV.

II. MODEL AND THEORY

Fig. 1 shows a schematic of the four mirror cavity considered in this work. Mirrors 1 and 2 are movable, each of which are driven by a coherent mechanical pump while

* palsp@uohyd.ernet.in

mirrors 3 and 4 are fixed. A pump laser of frequency ω_{pu} and a probe laser of frequency ω_{pr} enter the cavity from the left. The frequency of the cavity is taken to be ω_0 . Depending on which cavity is experiencing stronger field (as decided by the reflectivity and transmittivity of the beamsplitter and the optical length of each of the arms) will correspondingly exhibit stronger optomechanical coupling resulting from the radiation pressure, which results due to the incident input field inside the cavity. In this study, the parameters are chosen in such a manner as to render the field in arm 3 negligible [45].

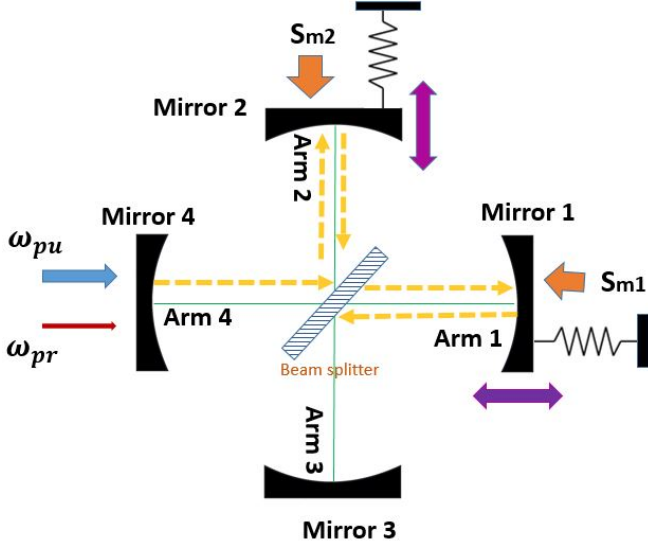


FIG. 1. Schematic diagram of a four mirror cavity with two movable mirror.

The Hamiltonian, describing various interactions that are considered here, is written in a rotating frame with frequency ω_0 in Eq. (1).

$$\begin{aligned}
 H = & \hbar \Delta_c a^\dagger a + \sum_{i=1,2} \left(\frac{p_i^2}{2m_i} + \frac{1}{2} m_i \omega_{mi}^2 x_i^2 - \hbar g a^\dagger a x_i \right) \\
 & + i \hbar \epsilon_{pu} (a^\dagger - a) + i \hbar \epsilon_{pr} (a^\dagger e^{-i\delta t} - a e^{i\delta t}) \\
 & - \sum_{i=1,2} s_{mi} x_i \cos(\delta t + \phi_{mi})
 \end{aligned} \quad (1)$$

Here a and a^\dagger are the bosonic operators of the cavity field, p_i and x_i are the momentum and position variables of the two movable mirrors each of which are modeled as simple harmonic oscillators, with frequency ω_{mi} , effective mass m_i and mechanical decay rate γ_{mi} with i taking the values 1,2. The pump (probe) amplitude ϵ_{pu} (ϵ_{pr}) is related to the input pump (probe) power P_{pu} (P_{pr}) as $\epsilon_{pu} = \sqrt{2\kappa P_{pu}/\hbar\omega_{pu}}$ ($\epsilon_{pr} = \sqrt{2\kappa P_{pr}/\hbar\omega_{pr}}$). The optomechanical coupling constant g is given by $g = \omega_{pu}/(L_4 + L_1 t^2 + L_2 r^2)$ where L_i ($i = 1,4$) are the respective arm lengths of the four mirror setup with r and t the reflection and transmission coefficients of the

beam splitter. The quantities s_{mi} and ϕ_{mi} ($i = 1,2$) are the amplitude and phase of the coherent mechanical drive.

It is often convenient to work with dimensionless position and momentum operators. We now define the dimensionless position and momentum operators for each of the two mirrors (Eq. (2)) and rewrite the Hamiltonian in terms of these operators as given by Eq. (3).

$$x_i = \sqrt{\frac{\hbar}{m_i \omega_{mi}}} Q_i \quad \text{and} \quad p_i = \sqrt{m_i \hbar \omega_{mi}} P_i \quad (2)$$

$$\begin{aligned}
 H = & \hbar \Delta_c a^\dagger a + \sum_{i=1,2} \frac{\hbar \omega_{mi}}{2} (P_i^2 + Q_i^2) - \hbar \sum_{i=1,2} G_i a^\dagger a Q_i \\
 & + i \hbar \epsilon_{pu} (a^\dagger - a) + i \hbar \epsilon_{pr} (a^\dagger e^{-i\delta t} - a e^{i\delta t}) \\
 & - \sum_{i=1,2} S_{mi} Q_i \cos(\delta t + \phi_{mi})
 \end{aligned} \quad (3)$$

Here the first term describes the cavity field energy with the cavity detuning given by $\Delta_c = \omega_0 - \omega_{pu}$ and the second term is the energy of the two mechanical oscillators. The third term describes the optomechanical interaction arising due to the coupling between the two mechanical oscillators and the cavity field. The effective coupling coefficient between cavity field and mirror 1 and 2 respectively are given by $G_1 = t^2 g \sqrt{\hbar/m_1 \omega_{m1}}$ and $G_2 = r^2 g \sqrt{\hbar/m_2 \omega_{m2}}$. The fourth and fifth terms describe the interaction between the cavity field and the input pump and probe fields respectively, with $\delta = \omega_{pr} - \omega_{pu}$, the pump - probe detuning. The last term describes the mechanical pumping energy applied to each movable mirror, with the driving parameter S'_{mi} defined by $S'_{mi} = s_{mi} \sqrt{\hbar/m_i \omega_{mi}}$ ($i=1,2$).

We denote the expectation values of each of the operators \hat{a} , \hat{Q} and \hat{P} with $\langle a \rangle$, $\langle Q \rangle$ and $\langle P \rangle$ respectively. Using the Hamiltonian given in Eq. (3), we derive the equations that describe the dynamical behaviour of these operator expectation values in Heisenberg picture, as follows.

$$\begin{aligned}
 \frac{d\langle a \rangle}{dt} = & -i \Delta_c \langle a \rangle + \epsilon_{pu} + \epsilon_{pr} e^{-i\delta t} + i G_1 \langle a \rangle \langle Q_1 \rangle \\
 & + i G_2 \langle a \rangle \langle Q_2 \rangle - \kappa \langle a \rangle \\
 \frac{d\langle Q_i \rangle}{dt} = & \omega_{mi} \langle P_i \rangle, (i = 1, 2) \\
 \frac{d\langle P_i \rangle}{dt} = & -\omega_{m1} \langle Q_i \rangle + G_i \langle a^\dagger \rangle \langle a \rangle - \gamma_i \langle P_i \rangle \\
 & + \frac{S'_{mi}}{\hbar} \cos(\delta t + \phi_{mi}), (i = 1, 2).
 \end{aligned} \quad (4)$$

In the above equations, κ is the cavity decay rate. In obtaining the above equations of motion, the mean field assumption $\langle MN \rangle = \langle M \rangle \langle N \rangle$ for the relevant operators has been used. Next, each of the variables is separated into a steady state solution and a small fluctuation

around its steady state value, i.e., $\hat{x} = x_s + \delta\hat{x}$. By substituting the same in each of the above equations, we can obtain the steady state solutions (Eq. (5)) as well as the equations of motion for the fluctuations in each of these

operators. The steady state solutions are given by

$$\begin{aligned} P_{is} &= 0, (i = 1, 2) \\ a_s &= \frac{\epsilon_{pr}}{\kappa + i\Delta} \\ Q_{is} &= \frac{G_i |a_s|^2}{\omega_{mi}}, (i = 1, 2) \end{aligned} \quad (5)$$

where $\Delta = \Delta_c - G_1 Q_1 - G_2 Q_2$. The equations of motion for the fluctuations in each of the operators are obtained as

$$\left(\frac{d}{dt} + (\kappa + i\Delta_c)\right)\delta a = \epsilon_{pr} e^{-i\delta t} + iG_1(Q_{1s}\delta a + a_s\delta Q_1) + iG_2(a_s\delta Q_2 + Q_{2s}\delta a) \quad (6)$$

$$\left(\frac{d^2}{dt^2} + \gamma_1 \frac{d}{dt} + \omega_{m1}^2\right)\delta Q_1 = G_1\omega_{m1}(a_s^*\delta a + a_s\delta a^*) + \frac{S'_{m1}\omega_{m1}}{\hbar} \cos(\delta t + \phi_{m1}) \quad (7)$$

$$\left(\frac{d^2}{dt^2} + \gamma_2 \frac{d}{dt} + \omega_{m2}^2\right)\delta Q_2 = G_2\omega_{m2}(a_s^*\delta a + a_s\delta a^*) + \frac{S'_{m2}\omega_{m2}}{\hbar} \cos(\delta t + \phi_{m2}). \quad (8)$$

We next use the ansatz

$$\delta X_i = X_i^- e^{-i\delta t} + X_i^+ e^{i\delta t}, (i = 1, 2), \quad (9)$$

for each of the variables and substitute this into the equations of motion for the fluctuations and group the coefficients of like-terms to obtain the solutions for the rel-

evant quantities of interest. For example, the term a_1^- is of interest in obtaining the anti-Stokes component of the output field from the cavity. In particular, the real part of anti-Stokes field is given by $Re(\eta_{as}) = Re(2\kappa a_1^- / \epsilon_{pr})$ [35]. The resulting equations for the fluctuations in the relevant variables are obtained as

$$(\kappa + i(\Delta - \delta))a_1^- = \epsilon_{pr} + iG_1 a_s Q_1^- + iG_2 a_s Q_2^- \quad (10)$$

$$(\kappa + i(\Delta + \delta))a_1^+ = iG_1 a_s Q_1^+ + iG_2 a_s Q_2^+ \quad (11)$$

$$(\omega_{m1}^2 - i\gamma_1\delta - \delta^2)Q_1^- = G_1\omega_{m1}(a_s^*a_1^- + a_s(a_1^+)^*) + \frac{S'_{m1}\omega_{m1}}{2\hbar} e^{-i\phi_{m1}} \quad (12)$$

$$(\omega_{m1}^2 + i\gamma_1\delta - \delta^2)Q_1^+ = G_1\omega_{m1}(a_s^*a_1^+ + a_s(a_1^-)^*) + \frac{S'_{m1}\omega_{m1}}{2\hbar} e^{+i\phi_{m1}} \quad (13)$$

$$(\omega_{m2}^2 - i\gamma_2\delta - \delta^2)Q_2^- = G_2\omega_{m2}(a_s^*a_1^- + a_s(a_1^+)^*) + \frac{S'_{m2}\omega_{m2}}{2\hbar} e^{-i\phi_{m2}} \quad (14)$$

$$(\omega_{m2}^2 + i\gamma_2\delta - \delta^2)Q_2^+ = G_2\omega_{m2}(a_s^*a_1^+ + a_s(a_1^-)^*) + \frac{S'_{m2}\omega_{m2}}{2\hbar} e^{+i\phi_{m2}}, \quad (15)$$

the solutions of which are obtained as

$$Q_2^- = \frac{\epsilon_{pr} a_s^* G_2 \chi_2(\delta) \alpha + 2\Delta \chi_2(\delta) G_1 G_2 |a_s|^2 Q_1^- + S_{m2} \chi_2(\delta) \alpha \beta e^{-i\phi_{m2}}}{\alpha \beta - 2G_2^2 |a_s|^2 \chi_2(\delta) \Delta} \quad (16)$$

$$Q_1^- = \frac{\alpha \chi_1(\delta) [\epsilon_{pr} a_s^* G_1 (d_2 + 2\Delta G_2^2 |a_{2s}|^2 \chi_2(\delta)) + \beta S_{m1} e^{-i\phi_{m1}} d_2] + \alpha \beta \chi_1(\delta) \chi_2(\delta) 2\Delta G_1 G_2 |a_{2s}|^2 S_{m2} e^{-i\phi_{m2}}}{d_1 d_2 - 4\Delta^2 G_1^2 G_2^2 |a_s|^4 \chi_1(\delta) \chi_2(\delta)} \quad (17)$$

$$a_1^- = \frac{\epsilon_{pr} + iG_1 a_s Q_1^- + iG_2 a_s Q_2^-}{\kappa + i(\Delta - \delta)} \quad (18)$$

Each of the hitherto undefined quantities that appear in the above solutions are defined by

$$\alpha = (\kappa - i(\Delta + \delta)); \quad \beta = (\kappa + i(\Delta - \delta)); \quad d_1 = \alpha\beta - 2G_1^2 |a_s|^2 \chi_1(\delta)\Delta; \quad d_2 = \alpha\beta - 2G_2^2 |a_s|^2 \chi_2(\delta)\Delta;$$

$$\Delta = \Delta_c - G_1 Q_1 - G_2 Q_2; \quad S_{mi} = \frac{S'_{mi}}{2\hbar}, (i = 1, 2); \quad \chi_1(\delta) = \frac{\omega_{m1}}{\omega_{m1}^2 - i\gamma_1\delta - \delta^2} \quad \text{and} \quad \chi_2(\delta) = \frac{\omega_{m2}}{\omega_{m2}^2 - i\gamma_2\delta - \delta^2}. \quad (19)$$

In the next section we present numerical simulations of the results for the real part of the generated anti-Stokes field as a function of the normalized probe detuning, for a wide range of parameters and discussion of the results.

III. RESULTS AND DISCUSSION

Here we focus on a study of the generated anti-stokes field (η_{as}) in the four mirror cavity, for a wide range of values of the input parameters.

As shown in Fig. 2, when the pump field of frequency ω_{pu} interacts with the mechanical mirror of frequency, say, Ω , absorption and emission of phonons creates the anti-Stokes field ($\omega_{pu} + \Omega$) and the Stokes field ($\omega_{pu} - \Omega$) respectively [44]. If the frequency of pump laser is red-detuned (tuned below the resonance frequency of cavity exactly by an amount Ω), then the anti-Stokes field becomes resonant with the cavity field and therefore gets enhanced, at the cost of suppression of the Stokes field, as now the Stokes field is far removed from resonance.

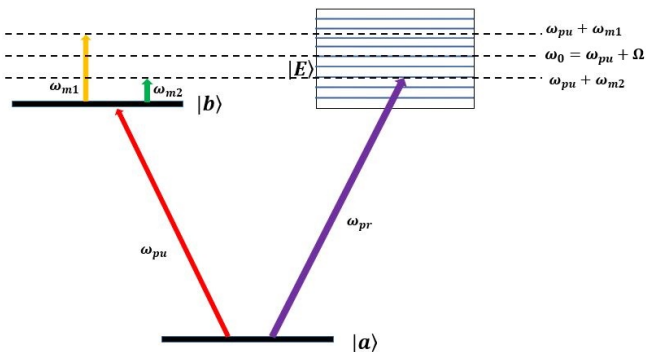


FIG. 2. Schematic illustration of frequencies used in obtaining Fano line shapes.

Ugo Fano, in a seminal paper [1], first described the asymmetric profile resulting in Rydberg spectral atomic lines and provided a detailed explanation of this feature arising due to resonant destructive interference between two transition pathways. In particular, one observes a minimum with an accompanying maximum very close to it, which is known by the name Fano resonance. Inside the four mirror cavity, when the frequency of the probe beam is tuned to that of the generated anti-Stokes field, destructive interference between these two fields gives rise to Fano-like resonance. As shown in Fig.2, interference takes place between the two transition pathways $|a\rangle \rightarrow |E\rangle$ and $|a\rangle \rightarrow |b\rangle \rightarrow |E\rangle$, where $|E\rangle$ represents a continuum of states (arising from the continuously tunable probe beam). Thus, when $\omega_{pr} = \omega_{pu} + \omega_{m1}$, destructive interference between the two fields (anti-Stokes and the probe) leads to a Fano-like resonance. Availability of two oscillating mirrors, which can be tuned independently of each other, at frequencies ω_{m1} and ω_{m2} respectively, provides two transition pathways from state $|b\rangle$ to

the continuum $|E\rangle$. A suitable choice of these parameters gives rise to a double Fano-like resonance. For instance, choosing the mechanical oscillation frequency of both the mirrors to be equal ($\omega_{m1} = \omega_{m2}$) results in superposition of the two resonances. Under this condition, the resulting Fano-like profile can be modified, giving rise to novel features, by tuning the amplitude and phase of the coherent mechanical pump. These features are illustrated in the following figures.

In this study, we have considered a truly macroscopic 4-mirror cavity, with the following parameters. Each of the cavity lengths $L_i = 35$ mm, ($i = 1, 4$), the effective pump laser detuning $\Delta = \Omega = 2\pi \times 10^7$ Hz, the cavity decay rate $\kappa = 2\pi \times 10^6$ MHz, mechanical damping rate of each mirror $\gamma_{mi} = 2\pi \times 10^4$ Hz ($i = 1, 2$), mass of each mirror $m_i = 14.5$ g, ($i = 1, 2$), and the pump power $P_{pu} = 10$ μ W respectively. It is to be noted that the parameters used in this study have been obtained from a careful survey of existing literature on macroscopic hybrid optomechanical systems [46–58]. Due to the macroscopic nature of the parameters of the four-mirror setup, the optomechanical coupling is very weak to show any observable optomechanical effects such as the optomechanically induced transparency, the Fano resonances which were earlier reported in microscopic cavities [35, 45]. This problem can however be circumvented by application of very nominal coherent driving field, resulting in observable optomechanical effects. In the following, we present numerical results for the real part of the anti-Stokes field for a variety of parameters, the details of which are contained in each of the figures, and demonstrate the significant role played by the amplitude and phase of the coherent mechanical drive, in observing the novel features reported here.

In the analytical expressions that were obtained in the previous section, the optomechanical interaction terms appear to several orders of the coupling parameter G . However, as the present OM system which has very weak optomechanical coupling, owing to its macroscopic nature as determined by the parameters that were considered, the quadratic and higher order terms result in negligible contribution to the features that are observed. We therefore neglect the higher order optomechanical interaction terms and retain only the linear terms in the interaction strength G . This gives rise to considerable simplification in the expression for a_1^- , which is obtained after neglecting all components containing second and higher order terms of effective OM coupling strength G_i ($i = 1, 2$), as shown below. It is to be noted that the scheme proposed here, involving the coherent mechanical driving of the mirrors, enhances the optomechanical interaction giving rise to observable effects, even at very nominal effective mechanical driving amplitudes S_{mi} ($i = 1, 2$).

$$a_1^- = \frac{\epsilon_{pr} + iG_1 a_s S_{m1} \chi_1(\delta) e^{-i\phi_{m1}} + iG_2 a_s S_{m2} \chi_2(\delta) e^{-i\phi_{m2}}}{\kappa + i(\Delta - \delta)} \quad (20)$$

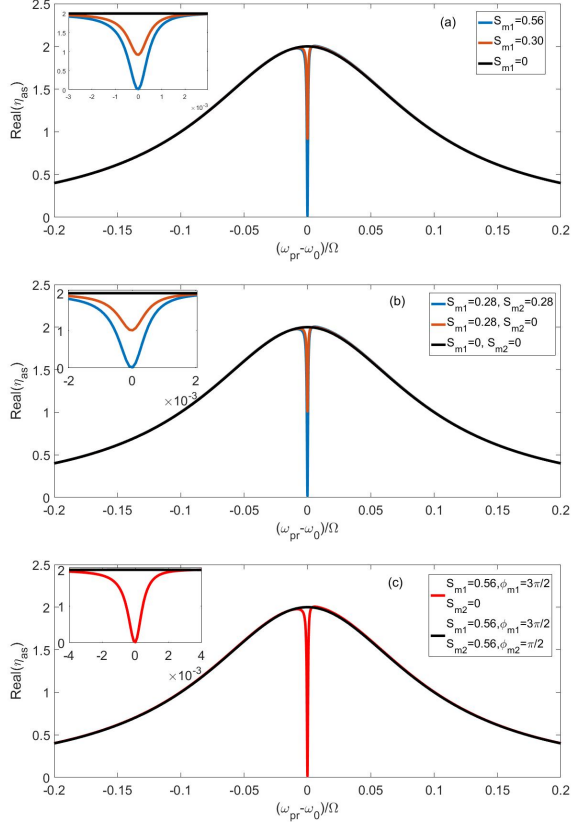


FIG. 3. Real part of anti-Stokes field as a function of normalized probe detuning for $\omega_{m1} = \Omega$, $\phi_{m1} = 3\pi/2$, (a) $S_{m1} = 0.56$ (blue), $S_{m1} = 0.30$ (red), $S_{m1} = 0$ (black) and $S_{m2} = 0$; (b) $S_{m1} = S_{m2} = 0.28$ (blue), $S_{m1} = 0.28$, $S_{m2} = 0$ (red), $S_{m1} = S_{m2} = 0$ (black); (c) $S_{m1} = 0.56$, $S_{m2} = 0$ (red), $S_{m1} = S_{m2} = 0.56$, $\phi_{m2} = \pi/2$ (black).

This expression can be simplified further by assuming $G_1 = G_2 = G$, $\chi_1 = \chi_2 = \chi$ resulting in the following.

$$a_1^- = \frac{\epsilon_{pr} + A(S_{m1}e^{-i\phi_{m1}} + S_{m2}e^{-i\phi_{m2}})}{\kappa + i(\Delta - \delta)}, \quad (21)$$

where A appearing in the above equation is given by $A = iG a_s \chi(\delta)$. We now study the behaviour of output spectrum for various combinations of amplitudes and phases of the two coherent mechanical pumps. At first, we look at the case when $\phi_{m1} = \phi_{m2} = 3\pi/2$.

Taking $\Delta = \delta = \Omega$, it is observed that a phase of $3\pi/2$ gives rise to OMIT at the line center. It is further seen that the strength of OMIT feature (as quantified by how close the dip is to its zero value) is proportional to the amplitude of the coherent mechanical pump which is illustrated in Fig. 3(a). Absence of mechanical driving i.e., $S_{m1} = 0$ (black), shows absence of OMIT at the line center. Introducing a small effective driving amplitude of $S_{m1} = 0.30$ (red) results in a dip at the line center, which indicates transmission of the probe beam on resonance. With further increase in the

amplitude, $S_{m1} = 0.56$ (blue) one observes a complete transmission of probe beam. The destructive interference between the probe beam and the anti-Stokes field when $\omega_{pr} = \omega_{pu} + \omega_{m1}$ gives rise to OMIT at the line center corresponding to $\omega_{m1} = \Omega$. The results of Fig. 3 show that an increase in the strength of mechanical pump gives rise to an enhancement in probe transmission, leading to complete transmission (OMIT) for a particular value of this parameter.

In Fig. 3(b), the absence of dip at the line center in the black curve shows clearly that OM effects are not present when the mechanical driving field is not applied, i.e., $S_{m1} = S_{m2} = 0$. Introduction of a small mechanical pump of amplitude $S_{m1} = 0.28$ on mirror 1, with $\omega_{m1} = \Omega$, gives rise to a dip at the line center, as seen in the red curve, showing clearly the generation of OMIT. Further inclusion of mechanical pump of the same amplitude ($S_{m2} = 0.28$) on mirror 2, with both the phases held at the same value, i.e., $\phi_{m1} = \phi_{m2} = 3\pi/2$, gives rise to complete transparency of the probe beam at the line center (blue). This feature can be attributed as arising due to coherent addition of the OM contributions arising from each of the mechanical driving fields, which are at the same phase.

This can further be substantiated by exploring whether the effect will cancel out by tuning one of the mechanical driving fields completely out of phase with the second. This is indeed the case, as shown in Fig. 3(c), where the red curve shows complete transparency of probe beam at the line center, generated solely due to S_{m1} , at a phase $\phi_{m1} = 3\pi/2$. Introducing the second mechanical drive S_{m2} at a phase $\phi_{m2} = \pi/2$ provides another channel which destructively interferes to cancel out this OMIT effect as seen from the black curve. Thus, tuning the amplitude and phase of the coherent mechanical pumps gives a handle to control the generation of OMIT in a macroscopic cavity.

In the results presented so far, it was shown that OMIT is observed at the line center, when the phases of the mechanical driving fields were held at $3\pi/2$. It would be interesting to see the effect of varying the phase of the mechanical pump on the OMIT features. For this purpose, at first, we switch off one of the mechanical pumps, say $S_{m2} = 0$ and keep the amplitude S_{m1} fixed at a particular value of 0.56 and vary its phase ϕ_{m1} at intervals of $\pi/2$ and record the changes in the output spectrum which are illustrated in Fig. 4.

Fig. 4(a) illustrates the case when only one of the mechanical driving fields is turned on ($S_{m1} = 0.56$ and $S_{m2} = 0$) at a phase $\phi_{m1} = 3\pi/2$, with $Re(\eta_{as})$ reaching its minimum value at the line center, identical to the red curve in Fig. 3(c). Keeping all other parameters fixed, we now change the phase ϕ_{m1} of S_{m1} to $\pi/2$, which gives rise to a sharp increase in $Re(\eta_{as})$ at the line center as shown in Fig. 4(b) showing remarkable absorptive behaviour of the cavity at $\pi/2$ phase. Other possible interesting values of phase ϕ_{m1} are explored further. The phase $\phi_{m1} = 0$ results in a Fano-like lineshape as shown in Fig. 4(c) and

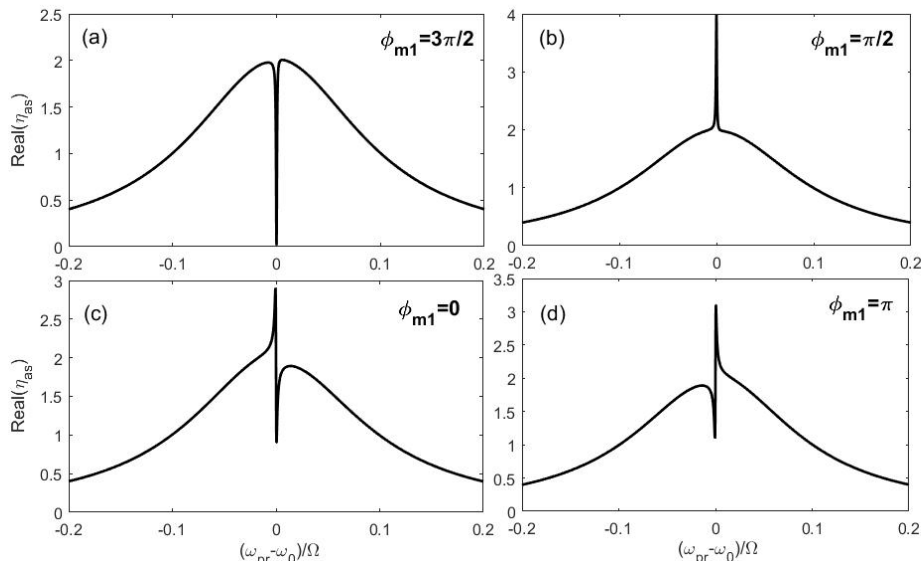


FIG. 4. Real part of anti-Stokes field as a function of normalized probe detuning for different values of phase ϕ_{m1} . (a) $\phi_{m1} = 3\pi/2$, (b) $\phi_{m1} = \pi/2$, (c) $\phi_{m1} = 0$, (d) $\phi_{m1} = \pi$

by changing the value of the phase to $\phi_{m1} = \pi$, gives rise to the lineshape as shown in Fig. 4(d), which is a mirror image of the previous case. Similar features have been observed in other optomechanical systems [59, 60]. These results clearly show the importance of coherent mechanical pump and its phase in controlling the spectral features of the generated fields. The sensitive changes in the behaviour of the system as a function of the phase of mechanical driving provide us a precision tool to detect the phase of an unknown harmonic force.

In the results presented so far, we have assumed that the oscillation frequencies of both the mirrors are equal to the effective cavity detuning, i.e. $\omega_{m1} = \omega_{m2} = \Omega$, the combination of which was giving rise to resonance at the line center. However, the ability to tune the oscillation frequencies of movable mirrors independently of one another can give rise to asymmetric lineshapes as shown in the Figures 5(a) and (b). Here we have tuned the oscillation frequency $\omega_{m1} = 1.2\Omega$, due to which the anti-Stokes field will destructively interfere with the probe beam whenever $\omega_{pr} = \omega_{pu} + 1.2\Omega$, as shown in Fig. 5(a). We observe occurrence of Fano-like resonance and a mirror image of the same, at a corresponding value of 0.2 of the normalized probe detuning, for phases $\phi_{m1} = 3\pi/2$ and $\pi/2$ respectively. The results presented for various combinations of the mechanical drive fields and their phases show clearly the interference effects between two transition pathways, in this case the fields generated at the probe frequency and at the anti-Stokes frequency. It is interesting to note that these features have not been observed so far in macroscopic cavities (due to the very weak optomechanical effects in such systems) and are resulting purely due to the introduction of coherent mechanical driving field(s).

Next, we consider the case when both the mechanical pumps (S_{m1} and S_{m2}) are switched on and degeneracy between oscillation frequencies of the mirrors is removed ($\omega_{m1} \neq \omega_{m2}$). This condition provides two distinct transition pathways ($(\omega_{pu} + \omega_{m1})$ and $(\omega_{pu} + \omega_{m2})$) to interfere with ω_{pr} , which gives rise to two resonances as clearly illustrated in Fig. 6. Here, in addition to the OMIT generated at the line center, a sharp resonance peak at $\delta/\Omega = 0.3$ ($\delta = \omega_{pr} - \omega_0$) is observed. The parameter considered here are $\omega_{m1} = \Omega$, $\phi_{m1} = 3\pi/2$ and $\omega_{m2} = \Omega + 0.3\Omega$, $\phi_{m2} = \pi$. Fig. 6, clearly shows that the strength (magnitude) of these OM features can be controlled by tuning the amplitude of the mechanical driving. When the effective amplitude $S_{m1} = 0.53$, we see a minima in the generated anti-Stokes field ($Re(\eta_{as})$) at the line center and a maxima at $\delta/\Omega = 0.3$ as shown by the blue curve in Fig. 6. With a decrease in the amplitudes of both mechanical pumps, $S_{m1} = 0.25$ and $S_{m2} = 0.89$, we see a considerable decrease in the strength of resonant curves at line center and at $\delta/\Omega = 0.3$, as can be seen from the red curve. The black curve illustrates the absence of any OM features as both the mechanical pumps are switched off, i.e., $S_{m1} = S_{m2} = 0$. It is to be mentioned that these OM features are generated in a macroscopic OM system with the introduction of coherent mechanical pump which has hitherto not been seen.

We next present our results on double Fano-like resonance lineshapes away from the line center, which can be tuned by introduction of mechanical driving fields and their phases. Such features have been widely studied in a different context in plasmonic structures [61, 62]. Very recently, these double Fano resonance lineshapes have been studied also in cavity optomechanical systems [35, 40]. In Fig.7 the resonant peak on the right to the

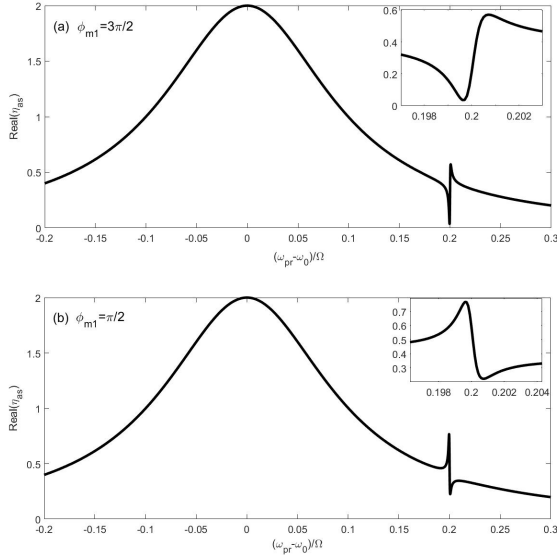


FIG. 5. Fano resonance in the real part of anti-Stokes field as a function of normalized probe detuning for $S_{m1} = 0.4$ and (a) $\phi_{m1} = 3\pi/2$; (b) $\phi_{m1} = \pi/2$.

line center appears due to the introduction of S_{m1} and the peak on the leftside results due to the introduction of S_{m2} . The parameters that were considered here are $\omega_{m1} = \Omega + 0.2\Omega$ and $\omega_{m2} = \Omega - 0.2\Omega$, due to which the resonance due to mirror 1 (S_{m1}) occurs at $\delta/\Omega = 0.2$ and that due to mirror 2 (S_{m2}) occurs at $\delta/\Omega = -0.2$. These resonances occur due to interference of probe beam and the anti-Stokes fields that are generated at $\omega_{pu} + \omega_{m1}$ and $\omega_{pu} + \omega_{m2}$ respectively. The location of these peaks can suitably be modified by tuning the mechanical frequency of the movable mirrors. Here, a mechanical pump S_{m1} with amplitude $S_{m1} = 0.85$ (Fig.7) is applied to generate a strong resonance peak on the left, whereas a slightly larger value of S_{m2} (0.93) is required to generate a resonance peak of similar height on the right side. This asymmetry arises from the fact that the resonance due to S_{m2} occurs when $\omega_{pr} = \omega_{pu} + 1.2\Omega$, which is far away from the pump laser frequency as compared to the resonance that occurs due to application of S_{m1} at $\omega_{pr} = \omega_{pu} + 0.8\Omega$. Therefore the closer we are to the pump laser frequency ω_{pu} , the smaller is the force that is needed to generate the OM resonance features and vice versa. One observes that by flipping the phase ϕ_{m2} from a value of 0 (red dashed curve) to π (black solid curve), the peak changes to a dip. The negative peak (red dashed) at $\delta/\omega_{m1} = 0.2$ corresponds to resonance amplification which can effectively be shifted to resonance absorption (positive peak) by adjusting the phase (ϕ_{m2}) of coherent mechanical pump. These features clearly show the important role played by the amplitude and phase of the coherent mechanical pump in tuning the absorption/amplification features as well as their positions.

Next we consider the case when the mechanical frequency of both oscillators are taken to be equal and

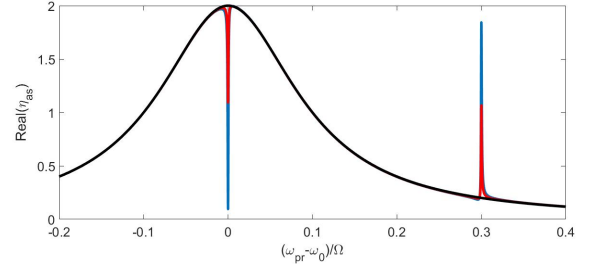


FIG. 6. Real part of anti-Stokes field as a function of normalized probe detuning ($\omega_{pr} - \omega_0$)/ Ω for $S_{m1} = 0.53$, $\phi_{m1} = 3\pi/2$ and $S_{m2} = 1.7$, $\phi_{m2} = \pi$ (blue); $S_{m1} = 0.25$, $\phi_{m1} = 3\pi/2$ and $S_{m2} = 0.89$, $\phi_{m2} = \pi$ (Red); $S_{m1} = 0$, $\phi_{m1} = 3\pi/2$ and $S_{m2} = 0$, $\phi_{m2} = \pi$ (black).

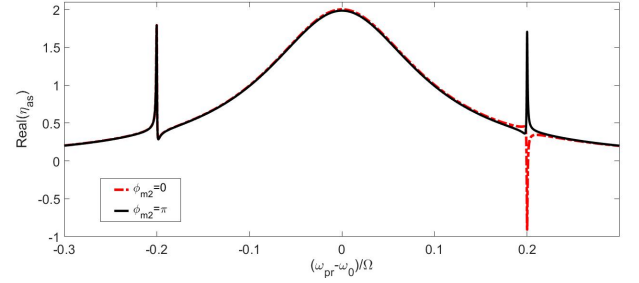


FIG. 7. Double Fano resonance in real part of anti-Stokes field as a function of normalized probe detuning, for $S_{m1} = 0.85$, $\omega_{m1} = 0.8\Omega$, $S_{m2} = 0.93$, $\omega_{m2} = 1.2\Omega$ and $\phi_{m1} = \phi_{m2} = 0$ (black solid curve); $\phi_{m1} = 0$ and $\phi_{m2} = \pi$ (red dashed curve).

tuned away from the cavity detuning ($\Delta_c = \Omega$) where $\omega_{m1} = \omega_{m2} \neq \Delta_c$, this enables one to control the resonance features by changing the phase of the mechanical pump. When both S_{m1} and S_{m2} have the same phase, namely, $\phi_{m1} = \phi_{m2} = \pi$, they constructively interfere to give an enhanced resonance peak at $\delta/\Omega = 0.3$ as shown by the blue curve in Fig. 8. Next, when the relative phase of the mechanical pumps, with strengths $S_{m1} = S_{m2} = 0.9$, is shifted from π to 2π or 0, destructive interference takes place between the two coherent processes which leads to total cancellation of the

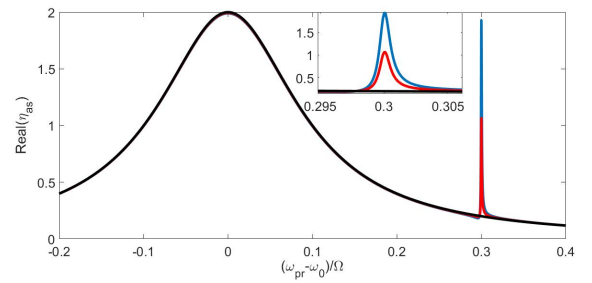


FIG. 8. Real part of anti-Stokes field vs normalized probe detuning for $S_{m1} = S_{m2} = 0.9$, $\phi_{m1} = \phi_{m2} = \pi$ (blue); $S_{m1} = 1.34$, $\phi_{m1} = \pi$, $S_{m2} = 0.45$, $\phi_{m2} = 0$ (red); $S_{m1} = S_{m2} = 0.9$, $\phi_{m1} = \pi$, $\phi_{m2} = 0$ (black).

Fano-like feature, resulting in the black curve. This situation amounts to effectively turning both the mechanical pumps off. We thus show that by tuning the relative phase between the two mechanical pumps, which are of equal magnitude, we can completely switch on/off the Fano-resonance. Taking their amplitudes unequal will result in further features in the Fano-resonance. For example, the red curve in Fig. 8 corresponds to unequal values of the mechanical driving fields, $S_{m1} = 1.34$ and $S_{m2} = 0.45$ with phases $\phi_{m1} = \pi$ and $\phi_{m2} = 0$, unlike the blue curve, in which both the mechanical drives were taken to have the same amplitude and phase.

IV. CONCLUSION

In this work we have shown how the OM features like optomechanically induced transparency and asymmetric

Fano line shapes can arise in four mirror macroscopic optomechanical cavities due to inclusion of coherent mechanical driving of two movable mirrors. We identify interfering pathways leading to the Fano resonances, which arise due to destructive interference between the input probe field and the generated anti-Stokes field in the hybrid optomechanical system considered here. We further show that these features can be efficiently controlled by changing the phase and amplitude of mechanical driving. For the degenerate case corresponding to the oscillation frequencies of both the mechanical oscillators being equal, we show that the phase can be used as a switch to generate interesting optomechanical effects. The freedom of tuning the two mechanical oscillators independent of each other, which is considered in this system, leads to the generation of tunable double Fano-like resonance. In conclusion, this work suggests the possibility of observing interesting tunable quantum effects at macroscopic scales, with the aid of coherent mechanical driving fields.

-
- [1] U. Fano, Phys. Rev. 124, 1866 (1961).
 [2] J. F. Scott, Rev. Mod. Phys. 46, 83128 (1974).
 [3] M. Hase, J. Demsar and M. Kitajima, Phys. Rev. B 74, 212301 (2006).
 [4] J. Faist, F. Capasso, C. Sitori, K. W. West and L. N. Pfeiffer, Nature 390, 589591 (1997).
 [5] M. Kroner, A. O. Govorov, S. Remi, B. Biedermann, S. Seidl, A. Badolato, P. M. Petroff, W. Zhang, R. Barbour, B. D. Gerardot, R. J. Warburton and K. Karrai, Nature 451, 311314 (2008).
 [6] B. Luk'yanchuk, N. I. Zheludev, S. A. Maier, N. J. Halas, P. Nordlander, H. Giessen and C. T. Chong, Nat. Mater. 9 707 (2010).
 [7] S. Fan, Appl. Phys. Lett. 80, 908910 (2002).
 [8] D. D. Smith, H. Chang, K. A. Fuller, A. T. Rosenberger and R. W. Boyd, Phys. Rev. A 69, 063804 (2004).
 [9] N. Liu, L. Langguth, T. Weiss, J. Kstel, M. Fleischhauer, T. Pfau and H. Giessen, Nature Mater. 8, 758762 (2009).
 [10] Y. Yoon, M. G. Kang, T. Morimoto, M. Kida, N. Aoki, J. L. Reno, Y. Ochiai, L. Mourokh, J. Fransson and J. P. Bird, Phys. Rev. X 2 021003 (2012).
 [11] S. Sasaki, H. Tamura, T. Akazaki and T. Fujisawa, Phys. Rev. Lett 103 266806 (2009).
 [12] A. C. Johnson, C. M. Marcus, M. P. Hanson and A. C. Gossard, Phys. Rev. Lett. 93 106803 (2004).
 [13] K. Kobayashi, H. Aikawa, A. Sano, S. Katsumoto, and Y. Iye, Phys. Rev. B 70 035319 (2004).
 [14] M. V. Rybin, A. B. Khanikaev, M. Inoue, K. B. Samusev, M. J. Steel, G. Yushin and M. F. Limonov, Phys. Rev. Lett. 103 023901 (2009).
 [15] M. Rahmani et al, Nano Lett. 12 2101 (2012).
 [16] W. Ding, B. Lukyanchuk and C. W. Qiu, Phys. Rev. A 85 025806 (2012).
 [17] S. Nojima, M. Usuki, M. Yawata and M. Nakahata, Phys. Rev. A 85 063818 (2012).
 [18] G. L. Shang, G. T. Fei, Y. Zhang, P. Yan, S. H. Xu, H. M. Ouyang, L. D. Zhang, Sci. Rep. 4 3601 (2014).
 [19] B. Gallinet and O. J. F. Martin, ACS Nano 5, 8999 (2011); Phys. Rev. B 83, 235427 (2011).
 [20] Y. Francescato, V. Giannini, and S. A. Maier, ACS Nano 6, 1830 (2012).
 [21] A. Artar, A. A. Yanik, and Hatice Altug, Nano Lett. 11, 3694 (2011).
 [22] R. Taubert, M. Hentschel, J. Kastel, and H. Giessen, ibid. 12, 1367 (2012).
 [23] N. Verellen, Y. Sonnefraud, H. Sobhani, F. Hao, V. V. Moshchalkov, P. Van Dorpe, P. Nordlander, S. A. Maier, Nano Lett. 09, 1663 (2009).
 [24] A. E. Miroshnichenko, S. Flach, and Y. S. Kivshar, Rev. Mod. Phys. 82, 2257 (2010).
 [25] J. Ye, F. Wen, H. Sobhani, J.B. Lassiter, P. Van Dorpe, P. Nordlander and N. J. Halas, Nano Lett. 12, 1660 (2012).
 [26] C. Wu, A. B. Khanikaev, and G. Shvets, Phys. Rev. Lett. 106, 107403 (2011).
 [27] Z. K. Zhou, X. N. Peng, Z. J. Yang, Z. S. Zhang, M. Li, X. R. Su, Q. Zhang, X. Shan, Q. Q. Wang, Z. Zhang, Nano Lett. 11, 49 (2011).
 [28] K. L. Lee, S. H. Wu, C. W. Lee, and P. K. Wei, Opt. Express 19, 24530 (2011).
 [29] G. Arkhipkin and Yu. I. Heller, Phys. Lett. A 98, 12 (1983).
 [30] O. A. Kocharovskaya and Ya. I. Khanin, Pisma Zh. Eksp. Teor. Fiz. 48, 581 (1988).
 [31] M. O. Scully, S. Y. Zhu, and A. Gavrielides, Phys. Rev. Lett. 62, 2813 (1989).
 [32] E. S. Fry, X. Li, D. Nikonov, G. G. Padmabandu, M. O. Scully, A. V. Smith, F. K. Tittel, C. Wang, S. R. Wilkinson, and S. Y. Zhu, ibid. 70, 3235 (1993).
 [33] G. S. Agarwal, S. L. Haan, and J. Cooper, Phys. Rev. A 29, 2552 (1984).
 [34] A. Barnthaler, S. Rotter, F. Libisch, J. Burgdorfer, S. Gehler, U. Kuhl, and H. J. Stockmann, Phys. Rev. Lett. 105, 056801 (2010).
 [35] K. Qu and G. S. Agarwal Phys. Rev. A 87, 063813 (2013).
 [36] M. J. Akram, F. Ghafoor, and F. Saif, J. Phys. B 48, 065502 (2015).
 [37] K. A. Yasira and W. M. Liu, Sci. Rep. 6, 22651 (2016).

- [38] S. Zhang, J. Li, R. Yu, W. Wang, and Y. Wu, *Sci Rep.* 7, 39781 (2017).
- [39] M. J. Akram, F. Ghafoor, M. M. Khan, and F. Saif, *Phys. Rev. A* 95, 023810 (2017).
- [40] C. Jiang, L. Jiang, H. Yu, Y. Cui, X. Li, and G. Chen, *Phys. Rev. A* 96, 053821 (2017).
- [41] T. Ramos, V. Sudhir, K. Stannigel, P. Zoller, and T. J. Kippenberg, *Phys. Rev. Lett.* 110, 193602 (2013).
- [42] H. Wang, X. Gu, Y. X. Liu, A. Miranowicz, and F. Nori, *Phys. Rev. A* 90, 023817 (2014).
- [43] H. Wang, X. Gu, Y. X. Liu, A. Miranowicz, and F. Nori, *Phys. Rev. A* 92, 033806 (2015).
- [44] G. S. Agarwal, *Quantum Optics* (Cambridge: Cambridge University Press) (2013).
- [45] F. Farman and A. Bahrapour, (Optical Society of America), paper JW2A.44. (2014).
- [46] K. C. Yellapragada, N. Pramanik, S. Singh, and P. Anantha Lakshmi, *Phys. Rev. A* 98, 053822 (2018).
- [47] P. Sekatski, M. Aspelmeyer, and N. Sangouard, *Phys. Rev. Lett.* 112, 080502 (2014).
- [48] S. Mancini, D. Vitali, and P. Tombesi, *Phys. Rev. Lett.* 80, 688 (1998).
- [49] L. F. Buchmann, L. Zhang, A. Chiruvelli, and P. Meystre, *Phys. Rev. Lett.* 108, 210403 (2012).
- [50] J. Q. Liao, Q. Q. Wu, and F. Nori, *Phys. Rev. A* 89, 014302 (2014).
- [51] T. P. Purdy, R. W. Peterson, and C. A. Regal, *Science* 339, 801 (2013).
- [52] D. Vitali, S. Mancini, L. Ribichini, and P. Tombesi, *J. Opt. Soc. Am. B* 20, 1054 (2003).
- [53] H. Tan, F. Bariani, G. Li, and P. Meystre, *Phys. Rev. A* 88, 023817 (2013).
- [54] S. Mancini, V. Giovannetti, D. Vitali, and P. Tombesi, *Phys. Rev. Lett.* 88, 120401 (2002).
- [55] F. Mueller, S. Heugel, and L. J. Wang, *Phys. Rev. A* 79, 031804 (2009).
- [56] J. T. Santos, J. Li, J. Ilves, C. F. Ockeloen-Korppi, and M. Sillanp, *New J. Phys.* 19, 103014 (2017).
- [57] N. Matsumoto, K. Komori, Y. Michimura, G. Hayase, Y. Aso, and K. Tsubono, *Phys. Rev. A* 92, 033825 (2015).
- [58] H. Suzuki, E. Brown, and R. Sterling, *Phys. Rev. A* 92, 033823 (2015).
- [59] J. Ma, C. You, L. Gang Si, H. Xiong, J. Li, X. Yang and Y. Wu, *Nature Scientific Reports*, *Scientific Reports* 5:11278 (2015).
- [60] W. Z. Jia, L. F. Wei, Yong Li, and Yu-xi Liu, *Phys. Rev. A* 91, 043843 (2015)
- [61] J. Wang, C. Fan, J. He, P. Ding, E. Liang, and Q. Xue, *Opt. Express* 21, 2236-2244 (2013).
- [62] B. Dana and A. Bahabad, *Optics Express* Vol. 24, No. 2 22334 (2016).